Vertically Stacked 2H-1T Dual-Phase MoS_2 Microstructures during Lithium Intercalation: A First Principles Study

S. Parida[1], A. Mishra[1], J. Chen[1], J. Wang[1], A. Dobley[2], C. B. Carter[3,4], and *A. M. Dongare*[1*†]

[1] Department of Materials Science and Engineering, and Institute of Materials Science, University of Connecticut, Storrs, CT 06269

[2] Yardney Division, EaglePicher Technologies LLC, East Greenwich, RI 02818

[3] Center for Integrated Nanotechnologies, Sandia National Laboratories, Albuquerque, NM 87123

[4] Department of Chemical & Biomolecular Engineering, University of Connecticut, Storrs, CT 06269,

Published in the Journal of the American Ceramic Society

103(11) 6603-14 (2020)

https://doi.org/10.1111/jace.17367

19 July 2020

[*] ORCID: http://orcid.org/0000-0003-3189-3588
[†] Corresponding author, electronic mail: dongare@uconn.edu

ABSTRACT

Layered transition-metal dichalcogenides (TMDs) have shown promise to replace carbon-based compounds as suitable anode materials for Lithium-ion batteries (LIBs) owing to facile intercalation and de-intercalation of lithium (Li) during charging and discharging, respectively. While the intercalation mechanism of Li in mono- and bi-layer TMDs have been thoroughly examined, mechanistic understanding of Li intercalation-induced phase transformation in bulk or films of TMDs is still largely unexplored. This study investigates possible scenarios during sequential Li intercalation and aims to gain a mechanistic understanding of the phase transformation in bulk MoS_2 using density functional theory (DFT) calculations. The manuscript examines the role of concentration and distribution of Li-ions on the formation of dual-phase 2H-1T microstructures that have been observed experimentally. The study demonstrates that lithiation would proceed in a systematic layer-by-layer manner wherein Li-ions diffuse into successive interlayer spacings to render local phase transformation of the adjacent MoS_2 layers from 2H-to-1T phase in the multilayered MoS_2. This local phase transition is attributed to partial ionization of Li and charge redistribution around the metal atoms and is followed by subsequent lattice straining. In addition, the stability of single-phase vs. multiphase intercalated microstructures, and the origins of structural changes accompanying Li-ion insertion are investigated at atomic scales.

Keywords: Layered materials, density functional theory (DFT), intercalation, phase transformation, lithiation

1. INTRODUCTION

Lithium-ion batteries (LIBs) are now widely used in consumer electronics, electric vehicles, and grid-scale energy applications as excellent energy-storage media.[1-4] With their impressive cyclic performance and high coulombic efficiency, layered graphite and spinel-type $Li_4Ti_5O_{12}$ are two of the most widely used anode materials in LIBs, with specific capacities of 372 mAh/g and 175 mAh/g, respectively.[5-7] Nonetheless, increasing demand for more efficient energy-to-electronic conversion devices, especially for hybrid vehicles, has led the search for new alternatives of anodic materials with higher capacities for LIBs. These include silicon, nano-carbons, alloys, metal oxides/sulfides/nitrides, and other layered materials of carbonaceous compounds, like graphite, graphene, and graphene oxides.[8-16]

Layered transition-metal dichalcogenides (TMDs) offer a high density of electrochemically active sites, fast ion transport, and hence, can lead to improved theoretical capacity and cycling stability of LIBs.[17-19] The large surface area and weak out-of-plane van der Waals (vdW) interactions in these materials, can overcome the current challenges of poor electronic conductivity and damaging volumetric fluctuations during the intercalation and de-intercalation. These materials, therefore, can find applications as various components of LIBs and sodium-ion-batteries (SIBs), including electrolytes, separators, as well as electrodes.[20-24] Interestingly, the first rechargeable LIB, marketed by Exxon in the 1970s, consisted of the TMD, TiS_2, as the cathode.[25] The large interlayer spacing between the TMD layers (typically ~0.6 nm)[26] can accommodate Li-ions without any significant change in the volume while charging and discharging. The optimization of layered TMDs for electrode application requires a fundamental understanding of the mechanisms of ion intercalation and the accommodation of related volumetric expansion and structural/phase stability of the layers.

Of the many other known TMDs, molybdenum disulfide (MoS_2) shows promise since it has a very high reversible capacity of 670 mAh/g for its semiconducting trigonal prismatic (2H) phase.[27] As a result, first-principles simulations have investigated the binding energies of Li in nanosheets and bulk MoS_2 as well as the diffusion energy barriers.[28-30] These studies also suggest Li intercalation on monolayer MoS_2 above a concentration of 40% of the available adsorption sites renders a phase transformation from the initial 2H to 1T phase,[31, 32] and has also been observed experimentally during Li intercalation.[33-35] Recent in-situ lithiation experiments[36] on thin film MoS_2 using high-resolution transmission electron microscopy (HRTEM) suggest the formation of several thin bands (typically 6-7 layers) of planar defects. The bands are observed to grow across the sample, parallel to the basal planes, and all of them have approximately the same thickness. These defect bands are likely to be associated with a local phase transformation of the 2H phase to the 1T phase that creates of 2H/1T interfaces during lithiation. If the defect bands are due to the formation of phase transformed thin layers of 1T phase MoS_2 distributed in a 2H matrix, then the mechanism here can be expected to be a local phenomenon; which is most likely dictated by Li concentration around a layer of MoS_2 (local concentration) rather than overall Li concentration across all the layers (global/total concentration). Similarly, experimental studies have suggested the composition dependence on the formation of coexisting 2H-1T microstructures during lithiation of 2H-MoS_2.[37, 38] The investigation of these local lithiation-induced phase transformation mechanisms in thin films of MoS_2, however, is very challenging using in situ transmission electron microscopy (TEM) experiments alone and ab-initio studies can help further the understanding.

The present study aims to gain a mechanistic understanding of the role of Li concentration and its distribution on the phase transformation behavior as well as co-existence of

a 2H-1T dual phase microstructure in bulk MoS_2 sheets using density functional theory (DFT) calculations. The calculations are carried out to investigate the various scenarios of intercalation given the availability of a large number of Li-ions and vdW gaps in the MoS_2 sheets. The different scenarios consider the intercalation process of a film of MoS_2 that is likely to have many Li-ions inserted into the several interlayer spacings that are available. The scenarios aim to address several questions that are yet unanswered and unravel the links between the intercalation mechanisms of Li-ions, their distribution, and the energetics of local phase transformation behavior. These questions include: Given an initial distribution of Li-ions in MoS_2 films, is it favorable for the new Li-ions to enter into a non-lithiated interlayer spacing, or does the Li-ion prefer to enter into a gap that already has an existing intercalated Li-ions? Similarly, if one interlayer spacing is lithiated, does it affect the intercalation behavior of Li-ions entering other interlayer spacings? In addition, the role of Li-ion concentration and the distribution of lithiated layers on the phase transformation behavior is unclear. As mentioned above, studies on monolayer MoS_2 sheets suggest a favorable transformation from the 2H to 1T phase when Li intercalation exceeds a critical concentration of 0.4.[31, 32, 39] However, it is not clear if this 2H-to-1T phase transformation will occur in thin films as soon as one of the interlayer spacing is intercalated to such a critical concentration of Li-ions, or when a critical concentration of Li-ions is reached across a few layers. Addressing these questions is the focus of this study to gain a mechanistic understanding of lithiation and phase transformation mechanisms in MoS_2 thin film/bulk structures. This study investigates these mechanisms of lithium intercalation, the role of distribution of intercalated layers, and the formation of dual-phase 2H-1T microstructures observed experimentally. As implied by previous experimental studies, and specifically shown by Janish *et al.* [36], the lithiated 2H phase of MoS_2 can serve as a precursor to obtain the 1T phase

during lithiation. In order to gain a mechanistic understanding of lithiation and the phase transformation behavior in thin films of MoS_2, the energetics of intercalation and the diffusion pathways are first identified in the bulk 2H phase for variations in the concentration of Li, followed by the investigation of the role of Li-ion concentration and distribution on the 2H-to-1T phase transformation behavior.

These results demonstrate that the distribution of lithiated layers (and not its overall concentration) plays a determining role in the 2H-to-1T phase transformation of MoS_2 sheets. The study establishes that lithiation would proceed in a systematic layer-by-layer manner. The insertion of the first Li-ion results in an increase in interlayer spacing between the adjoining MoS_2 layers. This increase in interlayer spacing creates preferential intercalation of the next Li-ion into the same interlayer spacing rather than insertion into a non-lithiated gap. The energetics of these competing mechanisms identify pathways for the insertion of successive Li-ions into the interlayer spacings. Calculations of the binding energy show that the preferred binding site for Li varies with the concentration of Li-occupied sites in the interlayer spacing of 2H-MoS_2. It also suggests that lithiation of consecutive interlayer spacings, wherein a 2H-MoS_2 layer is sandwiched between two Li layers, induces a local phase transformation of the sandwiched MoS_2 layer from 2H to 1T phase. The results demonstrate that the phase transformation is a local phenomenon that proceeds layer by layer and provides mechanistic insights into 2H-to-1T phase transformation behavior and the formation of dual-phase 2H-1T microstructures during Li intercalation in a thin film of MoS_2. Formation of certain skin depth of phase transformed 1T phase within 2H is expected as Li intercalation proceeds. Li diffusion is easier at the surface as compared to bulk of MoS_2 and phase transformation can thus be expected to start at the surface and proceed layer by layer into the bulk of MoS_2. This phenomenon can be exploited to tune the thickness of 1T layers

in MoS_2 microstructures by controlling Li distribution. The synergy between semiconducting 2H phase and phase transformed metallic 1T phase can find various applications.[40] Facile means to obtain 1T-MoS_2 from bulk 2H phase has been of interest owing to higher conductivity, better charge transfer ability and high reversible capacities etc.[41, 42] These properties make them suitable candidates for supercapacitors, rechargeable batteries, catalysis and surface-enhanced Raman scattering (SERS).[41-43] The computational details are provided in section II. The investigation of the intercalation behavior is discussed in section III, followed by the role of Li-ion concentration and distribution on the 2H-to-1T phase transformation behavior in section IV. The mechanisms of in-plane Li diffusion/growth of intercalated 2H or 1T layers are discussed in section V, followed by mechanistic insights on the effects of lattice straining are discussed in section VI.

II. Computational Details

All the first-principles calculations are carried out within the framework of DFT calculations using the Vienna *Ab-initio* Simulation Package (VASP).[44] A plane-wave basis is utilized to represent the wavefunction with an energy cut-off of 500 eV. The projector augmented-wave (PAW) method[45] is used to account for ion-electron interactions and electronic exchange correlations are expressed by generalized gradient approximation formulated by Perdew−Burke−Ernzerhof (GGA-PBE).[46] Reciprocal space for the bulk MoS_2 is sampled using $13 \times 13 \times 7$ gamma centered K-point mesh. Similarly, non-periodic layers or directional supercells are characterized with only one mesh point in the respective direction (e.g., monolayer MoS_2; $13 \times 13 \times 1$ K-mesh grid). The structural parameters for the cell are optimized using the conjugate gradient scheme until each component of the forces is ≤ 0.01 eV/Å. The bulk systems were optimized using ISIF3 tag of VASP, allowing cell shape, volume, and positions of atoms to

change in all directions. The Tkatchenko-Scheffler DFT method (DFT-TS)[47] is used to account for interlayer vdW interactions. Accounting for vdW interactions between different layers in TMDs becomes important as these interactions play a key role in the vertical stacking of individual layers. Wu et al.[48] highlighted the importance of considering vdW interactions in a DFT study of WSe_2 by computing strains required for transition from indirect-to-direct band gap with and without accounting for vdW interactions. The optimized lattice constants for the model systems considered are found to be a = 3.15 Å, c = 12.08 Å, $\alpha = 120^0$, $\gamma = 90^0$ for the 2H phase and a = 3.19 Å and the Mo-S distance is 2.41 Å, $\alpha = 120^0$, $\gamma = 90^0$ for the 1T phase (Figure S1 in supplementary material) and are in good agreement with experimental values and the DFT predicted values[49] reported in the literature. The binding energy (E_b) is calculated to identify the preferred binding sites for intercalated Li-ions using the equation:

$$E_b = E_{Li_xMoS_2} - (E_{MoS_2} + x\mu_{Li})$$

Here, $E_{Li_xMoS_2}$, E_{MoS_2}, and μ_{Li} correspond to the energies of Li-intercalated MoS_2, pristine MoS_2, and the Li-ion chemical potentials in its bulk BCC phase, respectively.

Electron and charge distribution or transfer analyses are performed by calculating electron localization function (ELF) and Bader charges. An ELF plot indicates the likelihood of finding an electron of the same spin given a reference electron. ELF map's value ranges between 0 and 1; 0 indicating delocalization or absence of an electron pair, while 1 indicates perfect localization of electron and 0.5 would represent a homogenous electron gas distribution. Bader analysis calculates total charges (core and valence) around an atom. These plots are useful in quantifying charge transfer between interacting atoms.

III. Layer-by-Layer Intercalation Behavior of Li-ions

A 10 × 1 × 1 supercell of 2H-MoS_2, as shown in Figure 1 (only a portion is shown), is used to investigate the intercalation behavior of Li-ions in bulk MoS_2. Li-ions are intercalated sequentially at various available sites in between 2H-MoS_2 layers. The mechanisms of intercalation are investigated based on the total energies of the system as well as the binding energies of Li-ions. The preferred intercalation sites for the first Li-ions are either an available (octahedral (O_h) and tetrahedral (T_d) sites. The energetics of subsequent Li intercalation is investigated here by considering two scenarios that can be expected in experiments, whether lithiation proceeds layer by layer or intercalation happens in a random manner.

The first scenario investigates if the intercalation of a one Li-ion into an interlayer spacing facilitates the insertion of subsequent Li-ions in the same gap. If not, the intercalation behavior is likely to be a random diffusion process that depends on the availability of interlayer spacings for subsequent Li-ions. Figure 1(a) illustrates this scenario with an existing Li-ion (middle image) and the case when the subsequent Li-ion is inserted in the same interlayer spacing (right image) is compared with the case when the subsequent Li-ion is inserted in an adjacent gap (left image). The systems are relaxed after the intercalation of the first Li-ion, which results in an expansion of the interlayer spacing by ~2%. The binding energy calculation suggests that second Li prefers to intercalate into the same interlayer spacing (where the first Li-ion resides) by 0.05 eV in comparison to intercalating into the next layer. Intercalation of additional Li-ions in the same interlayer spacing results in a further decrease in the binding energy, suggesting a preference for Li-ions to intercalate into already lithiated layers. Thus, the intercalation of the first Li-ion in an interlayer spacing is likely to result in subsequent lithiation of the same layer till all available sites are occupied. The binding energy per Li-ion as a function

of Li concentration indicates that the binding is preferred at the O_h site up to a coverage of 20%, exceeding which subsequent Li intercalation prefers to bind at the T_d site (Figure 1(b)). The finding is in agreement with the previously reported[30] dependence of Li intercalation site on Li-ion concentration and is attributed to the weakening of dispersive forces between S-atoms with the Li-ions as interlayer distances and in turn, distance between Li and the adjoining S-layers increases as more Li is intercalates into a layer.

The second scenario investigates if the occupation of all the available T_d sites in one vdW gap by Li-ions facilitates the intercalation of subsequent Li-ions prefer into the O_h sites in the same gap or an adjacent gap. Figure 2 illustrates the two possibilities with an existing lithiated vdW gap (middle image) and the case when the subsequent Li-ion is inserted in the same gap in the available O_h site (right image), and when the subsequent Li-ion is inserted in the adjacent gap (left image). Comparing the binding energy of Li, it is observed that after all the T_d sites in a layer are occupied; an additional Li would prefer to intercalate into an adjacent layer instead of supersaturating the same layer (with binding energy difference of ~1 eV). However, it can be expected that in the case of bulk MoS_2, Li-ions can also intercalate into any random interlayer spacing available. As a result, the calculated binding energy of randomly intercalated Li-ion is compared with that in the interlayer spacing adjacent to a lithiated layer (left image of Figure 2). The calculated energies indicate that lithiation in adjacent gaps is preferred over random intercalation by 0.04 eV.

The two scenarios discussed above indicate that the intercalation of a Li-ion creates a preference for the subsequent Li-ions to further intercalate into the same gap, till all the T_d sites in the layer are occupied and that, in turn, creates preferential sites for lithiation of the

neighboring interlayer spacings. Therefore, the lithiation of MoS_2 layers is likely to proceed layer-by-layer.

IV. Role of Li-ion Concentration and Distribution on 2H-1T Phase Transformation

The MoS_2 intercalation literature [31, 32, 39] implies that when the Li concentration exceeds 30-40%, a phase transformation occurs from 2H to 1T phase in the case of monolayer MoS_2. However, it is not known if such a transformation will occur in multilayered MoS_2 when the Li concentration exceeds the critical value. Such a phase transformation may likely require a critical concentration of Li across vertical layers. A 2H-to-1T phase transformation is energetically favorable when the energy of the lithiated-1T phase is lower than that of a lithiated-2H phase. To address this, DFT simulations are carried out using a $1 \times 1 \times 10$ supercells of 2H- and 1T-MoS_2. The interlayer spacings are lithiated one layer at a time leading to the formation of Li_xMoS_2; x ranges from 0 to 1 with a step size of 0.1 to investigate the energetics of lithiated structures for both the phases. Here it is assumed that intercalation proceeds one layer at a time based on the discussion of the intercalation mechanism above. Illustrative configurations for the lithiated 2H-MoS_2 structures for various Li concentrations are shown in Figure 3(a).

The calculated difference in energy between lithiated 2H and 1T-MoS_2 at various Li-ion layer concentrations is plotted in Figure 3(b). The plot shows that at Li concentrations exceeding 0.7, the lithiated 1T-MoS_2 structure has lower energy than the lithiated 2H-MoS_2. As a result, it is energetically favorable for the lithiated 2H phase to transform to the lithiated 1T phase. These calculations suggest that the critical Li-ion concentration for phase transformation of bulk MoS_2 is 0.7. Further, to understand the origin behind the observed 2H to 1T phase transformation in bulk MoS_2, the charge distribution and transfer analyses for the unlithiated and lithiated 2H and

1T-MoS_2 are performed. The charge redistribution around the S and Mo atoms with lithiation is observed in both the phases, as shown in Figure 4(a) and 4(b). Nevertheless, in the case of 2H-MoS_2 with the presence of Li, electron transfer is more restrained towards one of the adjoining S-layers in comparison to the other layer. It indicates the S atoms of the top layer gain more charges from Li, and thereby, less charge transfer from Mo to S happens in the top layer. In contrast, the bottom layer shows similar ELF as unlithiated 2H-MoS_2. The quantitative charge transfer estimation by Bader charge analysis also validates the biased gain of electrons by top layer S atoms, as shown in Figure 4(c). Furthermore, unlike the 2H phase in the case of lithiated 1T-MoS_2, the charge redistribution occurs such that S atoms in both the adjoining layers gain electrons equally, as evident from increased ELF value from 0 to ~0.1 throughout around Li-ions (Figure 4(b)). The charge transfer analysis also illustrates that all the S atoms gain (both Mo losses) similar charges, indicating the similar bonding of Li-ions with both layers (Figure 4(d)). Therefore, the increased bonding of Li in the 1T phase as compared to the tendency of Li to exhibit stronger bonding towards one of the neighboring MoS_2 layers compared to the other in the 2H phase is believed to be driving of lithiation driven phase transformation in MoS_2. This indicates that the phase transformation of the 2H phase to the 1T phase is only driven by the presence of Li ions. For a system where the concentration of Li is 0.7 (which is shown to be an energetically favorable condition for phase transformation) it unlikely that the unlithiated layers will also phase transform to the 1T phase. Therefore, it is reasonable to believe that phase transformation could proceed locally, with only the layers adjacent to incoming Li undergoing a phase change.

The same 10-layer system is considered to investigate the mechanism of phase transformation during the lithiation of consecutive layers, as shown in Figure 5(a). Lithiation is

carried out one layer at a time in the 2H phase, with the subsequent layer being adjacent to the previously lithiated layer. It is not clear if the phase transformation proceeds concurrently with lithiation. For example, after the lithiation of two successive layers in the 2H phase, is it likely that the MoS_2 layer sandwiched between the two Li layers phase transforms to the 1T phase that renders a Li-1T/2H hybrid structure. The suggested idea of the formation of a hybrid structure has also been observed in the experiments, showing the formation of a multiphase system during lithiation of 2H-MoS_2.[37, 50] As a result, the energy of a hybrid structure comprising of a lithiated 1T phase with the same number of Li layers in the matrix of a 2H phase is compared with that of the lithiated 2H structure. The initial 2H structure with one lithiated layer is shown as the left most structure in Figure 5(a), and the subsequent lithiation is carried out layer by layer. For each concentration of Li, the lithiated MoS_2 layers are phase transformed to the 1T phase to create 2H/1T hybrid structures with a lithiated 1T phase surrounded by an un-lithiated 2H phase. Such vertically stacked hybrid structures have stable 2H-1T interface normal to the *Z*-direction with interface energy as low as 0.068 J/m^2. The energy difference between the lithiated 2H phase and the hybrid 2H/1T phase as a function of Li concentration of lithiated layers is plotted in Figure 5(b). As discussed earlier, the structure is observed to be lower in energy for the 2H phase when only one interlayer spacing is lithiated. However, when two adjacent layers are lithiated, a transformation of the 2H-MoS_2 sandwiched between the Li layers to the 1T phase is observed to be energetically favorable. The observation hints towards the possibility of tuning the number and thickness of 2H and 1T layers in vertically stacked MoS_2 dual-phase microstructures by controlling Li distribution in the lattice. This could be interesting as the synergy between semiconducting 2H phase and metallic 1T phase can be utilized for various applications, e.g. catalysis.[40]

Further, the binding energy of Li decreases with an increase in Li content for both the structures, as shown in Figure 5(c). In the hybrid phase, the decrease in binding energy is significantly more than in the 2H phase. This is due to the formation of 1T layers in the hybrid phase, which binds Li more strongly than a 2H phase. It is also evident from binding energies of Li-ion at the 1T-2H interface (red curve) and Li within the 1T layers (blue curve); Li binds more strongly when present between two 1T layers than when present at the 1T-2H interface. Thus, phase transformation for a layer within the bulk structure can happen as soon as any layer is lithiated on both sides. A continued layer-by-layer lithiation of the adjacent interlayer spacings suggests that the transformation from 2H to 1T phase becomes more energetically favorable, as shown in Figure 5(b) and is associated with a decrease in the binding energy of the Li-ion. The simulations suggest that the fully lithiated 2H phase will completely transform to the lithiated 1T phase (Figure 5(b)), indicating phase transformation in bulk MoS_2 is locally driven. The charge redistribution during lithiation unveils the role of bonding/chemical behavior on the intercalation mechanism and phase transformation of bulk MoS_2. The ELF plots for the ten layered 2H and hybrid system with 0.2 concentration of Li (2H-$Li_{0.2}MoS_2$) are shown in Figure 6. The ELF for 2H-$Li_{0.2}MoS_2$ shows similar electron distribution as lithiated bulk 2H-MoS_2. In the case of the hybrid phase, the availability of only one phase transformed 1T layer leads to mixed bonding for Li with MoS_2 (at the 1T-2H interface), Li binds more strongly to 1T layer than to 2H layer and consequently, Li-ion binding at the interface is stronger than binding in between two 2H layers while it's lower than binding in between two 1T layers (as can be noted from the binding energy plot in Figure 5(c)).

The phase transformation from 2H to 1T phase in a single layer of MoS_2 proceeds via translation of S atom plane with respect to the other Mo and S planes, modifying co-ordination

of Mo atoms. However, in a multilayer system, there is added complexity of translation of the stacking of MoS_2 layers. For the phase transition from 2H to 1T phase, the stacking sequence changes from AB to AA type. Thus, different transition routes, as shown in Figure 7, are explored to find the lowest energy path leading to the transition. In particular, three scenarios are considered: first, S atoms within the layers translate to change the co-ordination around Mo, followed by the translation of MoS_2 layers to change the stacking sequence (Figure 7(a)); second, stacking sequence is altered followed by the change in co-ordination around Mo (Figure 7(b)), and third, change of stacking sequence as well co-ordination around Mo happen simultaneously, as shown in Figure 7(c).

Barrier calculations are performed for three scenarios as mentioned above, and the least resistance path is found when co-ordination around Mo and the stacking sequence change simultaneously (Figure 7(c)). Though, the transformation barrier is not significantly different along the 3 proposed routes (the difference is about 0.03 eV). The energy barrier for phase transformations with and without Li through the least resistance path is shown in Figure 8. Li intercalation significantly reduces the phase transformation barrier, as has been shown by studies on monolayer MoS_2[31]. Similarly, phase transformation barrier for partially lithiated structures carried out with layer closest incoming Li-ions phase transforming from 2H to 1T (favored route for layer by layer phase transformation in multilayered MoS_2 system) is found to be ~0.6 eV/MoS_2 (±0.2 eV) and is similar to the barrier for transformation for a fully lithiated system.

V. Collective Diffusion of Li-ions in Intercalated Layers

The experimental study[36] discussed earlier indicates that the defect bands formed during lithiation grow across the sample parallel to the basal planes. This suggests that the bands grow

by collective diffusion of Li-ions in the interlayer spacing at the lithiation front. However, it is not clear if this collective diffusion occurs in the intercalated 2H phase or the intercalated 1T phase. Therefore, it is essential to investigate the mechanisms and energetics of diffusion of intercalated Li layers in the 2H and 1T phase. Li-ions are intercalated at different available sites (O_h and T_d) in 1T and 2H phases (Figure S2 in supplementary material) assuming a complete lithiation. In the case of the 1T phase, the O_h site is found to be favorable for Li with a binding energy of -3.06 eV, whereas Li-ion in O_h for the 2H phase has a binding energy of -1.79 eV.

The simulations are carried out to determine the diffusion paths and corresponding energy barriers are calculated by translating the entire layer of Li-ions to the nearest equivalent binding sites by displacing them along the various possible routes, as shown in Figure 9(a) and (b) for bulk 2H- and 1T-MoS_2, respectively. For both phases, the shortest linear path for Li layer diffusion, denoted by RT1, is found to have a high energy barrier, with a barrier height of 0.36 and 1.01 eV for 2H and 1T phases, respectively (Figure 9(c)). Therefore, during intercalation and de-intercalation, Li diffusion would occur through alternative routes, such as RT3 for 2H-MoS_2 (through the O_h site) and RT2 for 1T phase (through the T_d site). The energy barrier for diffusion is significantly higher in 1T phase (0.8 eV per formula unit) than in 2H phase (0.24 eV per formula unit), which is attributed to the stronger binding of Li in the 1T phase. The observed trend agrees with the predicted behavior on Li migration on monolayer MoS_2.[29]

The results discussed here suggest that the collective diffusion of Li at the lithiation front is likely to be in the 2H phase. The phase transformation of the lithiated-2H layers to the 1T phase is likely to reduce this diffusion behavior due to the higher energy barrier. As a result, the formation of vertically stacked 2H-1T dual phase structures is likely to have diffusion of Li

layers in the 2H phase followed by a local 2H-to-1T phase transformation when the adjacent vdW gaps are lithiated.

VI. Mechanistic Insights on Formation of 2H-1T Dual Phase Microstructures

Further, to obtain an insight into the mechanics of the intercalation process, the effect of lattice straining must be explored. Li intercalation into a layer is seen to facilitate further intercalation into the same layer. Ease in further lithiation can be understood in terms of lattice straining, owing to electronic and steric factors, due to the expansion in interlayer spacing. It is akin to the opening of a channel for more lithium to enter the spacing. The preference for insertion of Li-ions in the same layer until all the T_d sites are occupied is indicative of intercalation preferring to proceed layer by layer in multilayer MoS_2. As two consecutive interlayer spacings are intercalated, the MoS_2 layer between then is likely to phase transform from 2H to 1T phase preferentially. This phase transformation, however, may be limited by the barrier of the phase transformation. Similarly, the small energy difference for Li intercalating into adjacent or distant layers, indicates that it would not be necessary for two Li layers to be adjacent to each other in a bulk MoS_2 for driving phase transformation. Nevertheless, in the experimental situation, the higher concentration of Li would lead to the possibility of consecutive lithiation for facilitating the phase transformation. Also, when the Li concentration exceeds 0.6, several MoS_2 layers would be lithiated on both sides, and thus, it is very likely that few layers would transform into the 1T phase locally.

The lattice expansion that relaxes the stresses developed due to steric and electronic repulsions is observed along the Z-direction because of the vdW stacking. The volumetric expansion in lithiated 2H and hybrid phase as a function of Li concentration is plotted in Figure

10. The vertically stacked 2H-1T microstructure shows different stacking depending upon if there are an even or odd number of 2H layers; this results in the zig-zag nature of the volumetric expansion curve. The distance between 1T and 2H layers at the interface is measured; in the case of even layers of 1T, the layers are 0.05 Å closer compare to an odd number of 1T layers. The ionic radius of the Li^+ ion is significantly smaller than the vdW gap; still, considerable lattice expansion is seen during the simulations. The volumetric expansion of ~6% can be expected upon full lithiation owing to a change in ionicity of the anion. A similar expansion of 4-6% in the Z-direction has also been reported in experimental studies as well during lithium cycling and has been attributed to a decrease in ionicity of Li with an increase in ion concentration.[51] A decrease in ionicity leads to an increase in the ionic radius of Li and explains the observed volumetric expansion. With a smaller interlayer spacing in the 1T phase, 2H-1T transformation lowers the straining, as compared to the scenario when there is no phase transformation accompanying lithiation. The findings also suggest that when the lattice is not allowed to expand during lithiation, larger stress will build up in the 2H phase than in vertically stacked 2H-1T microstructure, this could expedite phase transformation to lower the stresses developed due to lattice straining.

The results discussed here provide mechanistic insights in the formation of vertically stacked MoS_2 dual-phase microstructures given distribution of intercalated vdW gaps. While the simulations are carried out for Li-ion intercalation, the behavior is expected to be similar for could be observed for the intercalation of different ions like Na^+, K^+, and Mg^{2+} in multilayer TMDs. The results demonstrate the possibility of tuning the number and thickness of 2H and 1T layers by controlling the distribution of ions in the lattice to tailor the response in various applications.[38,40]

VII. Conclusions and Outlook

In summary, this comprehensive study investigates the mechanistic origin of phase transformation in bulk MoS_2 using first-principles calculations. The increase in the interlayer spacing when the concentration of Li exceeds 30% leads to a change in the preferential absorption site for Li intercalation. The reduction in binding energy with the inclusion of Li suggests lithiation could be favorable until all the tetrahedral sites in the interlayer spacing between two 2H-MoS_2 are occupied, followed by intercalation into adjacent vdW gaps. Once a layer of MoS_2 is sandwiched between two lithiated vdW gaps, it energetically favors to transform from 2H to 1T phase. Therefore, layer-by-layer lithiation and subsequently, a local 2H-to-1T phase transformation is preferred. These results suggest that there is no overall critical concentration of Li that is required to trigger the phase transformation in the bulk phase of MoS_2; as soon as a 2H-layer of MoS_2 is lithiated on both sides, the layer favors to transform to 1T. Thus, phase transformation is more reliant on Li-ion distribution, which determines local concentration near a layer of MoS_2, rather than the total concentration in multilayered MoS_2. The phase transformation during lithiation is due to the electronic redistribution around S atoms and is a stress release mechanism. The key finding of this study is that intercalation assisted phase transformation is a local phenomenon leading to the formation of vertically stacked 2H-1T dual-phase microstructures during partial Li intercalation. The results also suggest that a similar trend could be observed for the intercalation of different ions like Na^+, K^+, and Mg^{2+} in multilayer transition layer dichalcogenides. Such insights in the creation of vertically stacked dual-phase microstructures of TMDs during lithiation are essential in realizing their potential in energy storage applications.

IX. Acknowledgements

The authors acknowledge discussions with Drs Matt Janish, Manish Singh, Chanchal Ghosh, and Christine Cook. C. Barry Carter carries out his research at CINT, the Center for Integrated Nanotechnology, which is a User Facility supported by DOE at Sandia National Laboratories. This work is supported by the US NSF under grant no. DMR-1820565. This work is being supported by (NSF) grant no. 1820565 and CINT user proposal no. 2018BUO161. The authors would also like to acknowledge the resources from the UConn High Performance Computing (HPC) facility used to carry out this work.

References

1. Wang, Q, Mao, B, Stoliarov, SI, Sun, J. A review of lithium ion battery failure mechanisms and fire prevention strategies. *Prog. Energy Combust. Sci.* 2019; 73: 95-131 https://doi.org/10.1016/j.pecs.2019.03.002

2. Whittingham, MS. Ultimate Limits to Intercalation Reactions for Lithium Batteries. *Chem. Rev.* 2014; 114[23]: 11414-43 10.1021/cr5003003

3. Goodenough, JB, Park, K-S. The Li-Ion Rechargeable Battery: A Perspective. *J. Am. Chem. Soc.* 2013; 135[4]: 1167-76 10.1021/ja3091438

4. Wang, A, Kadam, S, Li, H, Shi, S, Qi, Y. Review on modeling of the anode solid electrolyte interphase (SEI) for lithium-ion batteries. *Npj Comput. Mater.* 2018; 4[1]: 15 10.1038/s41524-018-0064-0

5. Nonaka, T, Kawaura, H, Makimura, Y, Nishimura, YF, Dohmae, K. In situ X-ray Raman scattering spectroscopy of a graphite electrode for lithium-ion batteries. *J. Power Sources* 2019; 419: 203-07 https://doi.org/10.1016/j.jpowsour.2019.02.064

6. Liu, Z, Yu, Q, Zhao, Y, He, R, Xu, M, Feng, S, et al. Silicon oxides: a promising family of anode materials for lithium-ion batteries. *Chem. Soc. Rev.* 2019; 48[1]: 285-309 10.1039/C8CS00441B

7. Yazami, R, Touzain, P. A reversible graphite-lithium negative electrode for electrochemical generators. *J. Power Sources* 1983; 9[3]: 365-71 https://doi.org/10.1016/0378-7753(83)87040-2

8. Xu, B, Luo, Y, Liu, T, Zhang, Q, Lin, Y-H, Nan, C-W, et al. Ultrathin N-doped carbon-coated TiO_2 coaxial nanofibers as anodes for lithium ion batteries. *J. Am. Chem. Soc.* 2017; 100[7]: 2939-47 10.1111/jace.14822

9. Li, H, Wang, Z, Chen, L, Huang, X. Research on Advanced Materials for Li-ion Batteries. *Adv. Mater.* 2009; 21[45]: 4593-607 10.1002/adma.200901710

10. Huddleston, W, Dynys, F, Sehirlioglu, A. Nickel percolation and coarsening in sintered $Li_4Ti_5O_{12}$ anode composite. *J Am Ceram Soc.* 2020; 103: 4178- 4188. 10.1111/jace.17159

11. Wang, P, Gou, X-X, Xin, S, Cao, F-F. Facile synthesis of CuO nanochains as high-rate anode materials for lithium-ion batteries. *New J Chem.* 2019; 43[17]: 6535-39 10.1039/C9NJ01015G

12. Melchior, SA, Palaniyandy, N, Sigalas, I, Iyuke, SE, Ozoemena, KI. Probing the electrochemistry of MXene (Ti_2CT_x)/electrolytic manganese dioxide (EMD) composites as anode materials for lithium-ion batteries. *Electrochim. Acta* 2019; 297: 961-73 https://doi.org/10.1016/j.electacta.2018.12.013

13. Wu, H, Zhang, Z, Qin, M, Wang, Q, Cao, Z, Yu, Y, et al. Solution combustion synthesis of crystalline V_2O_3 and amorphous V_2O_3/C as anode for lithium-ion battery. *J. Am. Chem. Soc.* 2020; 103[4]: 2643-52 10.1111/jace.16962

14. Wang, Q, Huang, Y, Miao, J, Zhao, Y, Zhang, W, Wang, Y. Graphene-Supported Ce–SnS_2 Nanocomposite as Anode Material for Lithium-Ion Batteries. *J Am Ceram Soc.* 2013; 96[7]: 2190-96 10.1111/jace.12302

15. Su, W, Liang, Y, Tang, Y. Facile situ synthesis of C@SnO_2/Sn@rGO hybrid nanosheets as high performance anode materials for lithium-ion batteries. *J. Alloys Compd.* 2019; 801: 402-08 https://doi.org/10.1016/j.jallcom.2019.05.288

16. Seo, S-D, Lee, D-H, Shim, H-W, Lee, S, Kim, D-W. Enhanced Cycle Stability of Magnetite/Carbon Nanoparticles for Li Ion Battery Electrodes. *J Am Ceram Soc.* 2014; 97[5]: 1413-20 10.1111/jace.12905

17. Whittingham, MS. Chemistry of intercalation compounds: Metal guests in chalcogenide hosts. *Prog. Solid. State Ch.* 1978; 12[1]: 41-99 https://doi.org/10.1016/0079-6786(78)90003-1

18. Wang, H, Feng, H, Li, J. Graphene and Graphene-like Layered Transition Metal Dichalcogenides in Energy Conversion and Storage. *Small* 2014; 10[11]: 2165-81 10.1002/smll.201303711

19. Tao, K, Wang, X, Xu, Y, Liu, J, Song, X, Fu, C, et al. Engineering defect-enabled 3D porous MoS_2/C architectures for high performance lithium-ion batteries. *J Am Ceram Soc.* 2020; 103: 4453- 4462. 10.1111/jace.17082

20. Sriram, MA, Kumta, PN. Thio Sol–Gel Process for the Synthesis of Titanium Disulfide. *J Am Ceram Soc.* 1994; 77[5]: 1381-84 10.1111/j.1151-2916.1994.tb05422.x

21. Chhowalla, M, Shin, HS, Eda, G, Li, L-J, Loh, KP, Zhang, H. The chemistry of two-dimensional layered transition metal dichalcogenide nanosheets. *Nat. Chem.* 2013; 5: 263 10.1038/nchem.1589

22. Wan, J, Hao, Y, Shi, Y, Song, Y-X, Yan, H-J, Zheng, J, et al. Ultra-thin solid electrolyte interphase evolution and wrinkling processes in molybdenum disulfide-based lithium-ion batteries. *Nat. Commun.* 2019; 10[1]: 3265 10.1038/s41467-019-11197-7

23. Ullah, H, Noor-A-Alam, M, Shin, Y-H. Vacancy- and doping-dependent electronic and magnetic properties of monolayer SnS_2. *J Am Ceram Soc.* 2020; 103[1]: 391-402 10.1111/jace.16739

24. Lin, L, Lei, W, Zhang, S, Liu, Y, Wallace, GG, Chen, J. Two-dimensional transition metal dichalcogenides in supercapacitors and secondary batteries. *Energy Storage Mater.* 2019; 19: 408-23 https://doi.org/10.1016/j.ensm.2019.02.023

25. Whittingham, MS. Electrical Energy Storage and Intercalation Chemistry. *Science* 1976; 192[4244]: 1126 10.1126/science.192.4244.1126

26. Sen, UK, Mitra, S. High-Rate and High-Energy-Density Lithium-Ion Battery Anode Containing 2D MoS_2 Nanowall and Cellulose Binder. *ACS Appl. Mater. Interfaces* 2013; 5[4]: 1240-47 10.1021/am3022015

27. Bozheyev, F, Zhexembekova, A, Zhumagali, S, Molkenova, A, Bakenov, Z. MoS_2 nanopowder as anode material for lithium-ion batteries produced by self-propagating high-temperature synthesis. *Mater. Today: Proceedings* 2017; 4[3, Part A]: 4567-71 https://doi.org/10.1016/j.matpr.2017.04.031

28. Li, Y, Wu, D, Zhou, Z, Cabrera, CR, Chen, Z. Enhanced Li Adsorption and Diffusion on MoS_2 Zigzag Nanoribbons by Edge Effects: A Computational Study. *J. Phys. Chem. Lett.* 2012; 3[16]: 2221-27 10.1021/jz300792n

29. Sun, X, Wang, Z, Fu, YQ. Defect-Mediated Lithium Adsorption and Diffusion on Monolayer Molybdenum Disulfide. *Sci. Rep.* 2015; 5: 18712 10.1038/srep18712

30. Shuai, J, Yoo, HD, Liang, Y, Li, Y, Yao, Y, Grabow, LC. Density functional theory study of Li, Na, and Mg intercalation and diffusion in MoS_2 with controlled interlayer spacing. *Mater. Res. Express* 2016; 3[6]: 064001 10.1088/2053-1591/3/6/064001

31. Nasr Esfahani, D, Leenaerts, O, Sahin, H, Partoens, B, Peeters, FM. Structural Transitions in Monolayer MoS_2 by Lithium Adsorption. *J. Phys. Chem. C* 2015; 119[19]: 10602-09 10.1021/jp510083w

32. Shu, H, Li, F, Hu, C, Liang, P, Cao, D, Chen, X. The capacity fading mechanism and improvement of cycling stability in MoS_2-based anode materials for lithium-ion batteries. *Nanoscale* 2016; 8[5]: 2918-26 10.1039/C5NR07909H

33. Chrissafis, K, Zamani, M, Kambas, K, Stoemenos, J, Economou, NA, Samaras, I, et al. Structural studies of MoS_2 intercalated by lithium. *Mater. Sci. Eng., B* 1989; 3[1]: 145-51 https://doi.org/10.1016/0921-5107(89)90194-3

34. Jiao, Y, Mukhopadhyay, A, Ma, Y, Yang, L, Hafez, AM, Zhu, H. Ion Transport Nanotube Assembled with Vertically Aligned Metallic MoS_2 for High Rate Lithium-Ion Batteries. *Adv. Energy Mater.* 2018; 8[15]: 1702779 10.1002/aenm.201702779

35. Eda, G, Yamaguchi, H, Voiry, D, Fujita, T, Chen, M, Chhowalla, M. Photoluminescence from Chemically Exfoliated MoS_2. *Nano Lett.* 2011; 11[12]: 5111-16 10.1021/nl201874w

36. Janish, MT, Carter, CB. In situ TEM observations of the lithiation of molybdenum disulfide. *Scr. Mater.* 2015; 107: 22-25 https://doi.org/10.1016/j.scriptamat.2015.05.011

37. Py, MA, Haering, RR. Structural destabilization induced by lithium intercalation in MoS_2 and related compounds. *Can. J. Phys.* 1983; 61[1]: 76-84 10.1139/p83-013

38. Wang, H, Lu, Z, Xu, S, Kong, D, Cha, JJ, Zheng, G, et al. Electrochemical tuning of vertically aligned MoS_2 nanofilms and its application in improving hydrogen evolution reaction. *PNAS* 2013; 110[49]: 19701-06 10.1073/pnas.1316792110

39. Pandey, M, Bothra, P, Pati, SK. Phase Transition of MoS_2 Bilayer Structures. *J. Phys. Chem. C* 2016; 120[7]: 3776-80 10.1021/acs.jpcc.5b10904

40. Zhang, G, Liu, H, Qu, J, Li, J. Two-dimensional layered MoS_2: rational design, properties and electrochemical applications. *Energy Environ. Sci.* 2016; 9[4]: 1190-209 10.1039/C5EE03761A

41. Er, E, Hou, H-L, Criado, A, Langer, J, Möller, M, Erk, N, et al. High-Yield Preparation of Exfoliated 1T-MoS_2 with SERS Activity. *Chem. Mater.* 2019; 31[15]: 5725-34 10.1021/acs.chemmater.9b01698

42. Sun, D, Huang, D, Wang, H, Xu, G-L, Zhang, X, Zhang, R, et al. 1T MoS_2 nanosheets with extraordinary sodium storage properties via thermal-driven ion intercalation assisted exfoliation of bulky MoS_2. *Nano Energy* 2019; 61: 361-69 https://doi.org/10.1016/j.nanoen.2019.04.063

43. Acerce, M, Voiry, D, Chhowalla, M. Metallic 1T phase MoS_2 nanosheets as supercapacitor electrode materials. *Nat. Nanotechnol.* 2015; 10[4]: 313-18 10.1038/nnano.2015.40

44. Kresse, G, Hafner, J. Ab initio molecular dynamics for liquid metals. *Phys. Rev. B* 1993; 47[1]: 558-61 10.1103/PhysRevB.47.558

45. Blöchl, PE. Projector augmented-wave method. *Phys. Rev. B* 1994; 50[24]: 17953-79 10.1103/PhysRevB.50.17953

46. Perdew, JP, Burke, K, Ernzerhof, M. Generalized Gradient Approximation Made Simple [Phys. Rev. Lett. 77, 3865 (1996)]. *Phys. Rev. Lett.* 1997; 78[7]: 1396-96 10.1103/PhysRevLett.78.1396

47. Tkatchenko, A, Scheffler, M. Accurate Molecular Van Der Waals Interactions from Ground-State Electron Density and Free-Atom Reference Data. *Phys. Rev. Lett.* 2009; 102[7]: 073005 10.1103/PhysRevLett.102.073005

48. Wu, W, Wang, J, Ercius, P, Wright, NC, Leppert-Simenauer, DM, Burke, RA, et al. Giant Mechano-Optoelectronic Effect in an Atomically Thin Semiconductor. *Nano Lett.* 2018; 18[4]: 2351-57 10.1021/acs.nanolett.7b05229

49. Li, M, Shi, J, Liu, L, Yu, P, Xi, N, Wang, Y. Experimental study and modeling of atomic-scale friction in zigzag and armchair lattice orientations of MoS_2. *Sci. Technol. Adv. Mater.* 2016; 17[1]: 189-99 10.1080/14686996.2016.1165584

50. Julien, CM. Lithium intercalated compounds: Charge transfer and related properties. *Mater. Sci. Eng. R Rep.* 2003; 40[2]: 47-102 https://doi.org/10.1016/S0927-796X(02)00104-3

51. Stephenson, T, Li, Z, Olsen, B, Mitlin, D. Lithium ion battery applications of molybdenum disulfide (MoS_2) nanocomposites. *Energy & Environ. Sci.* 2014; 7[1]: 209-31 10.1039/C3EE42591F

FIGURES AND FIGURE CAPTIONS

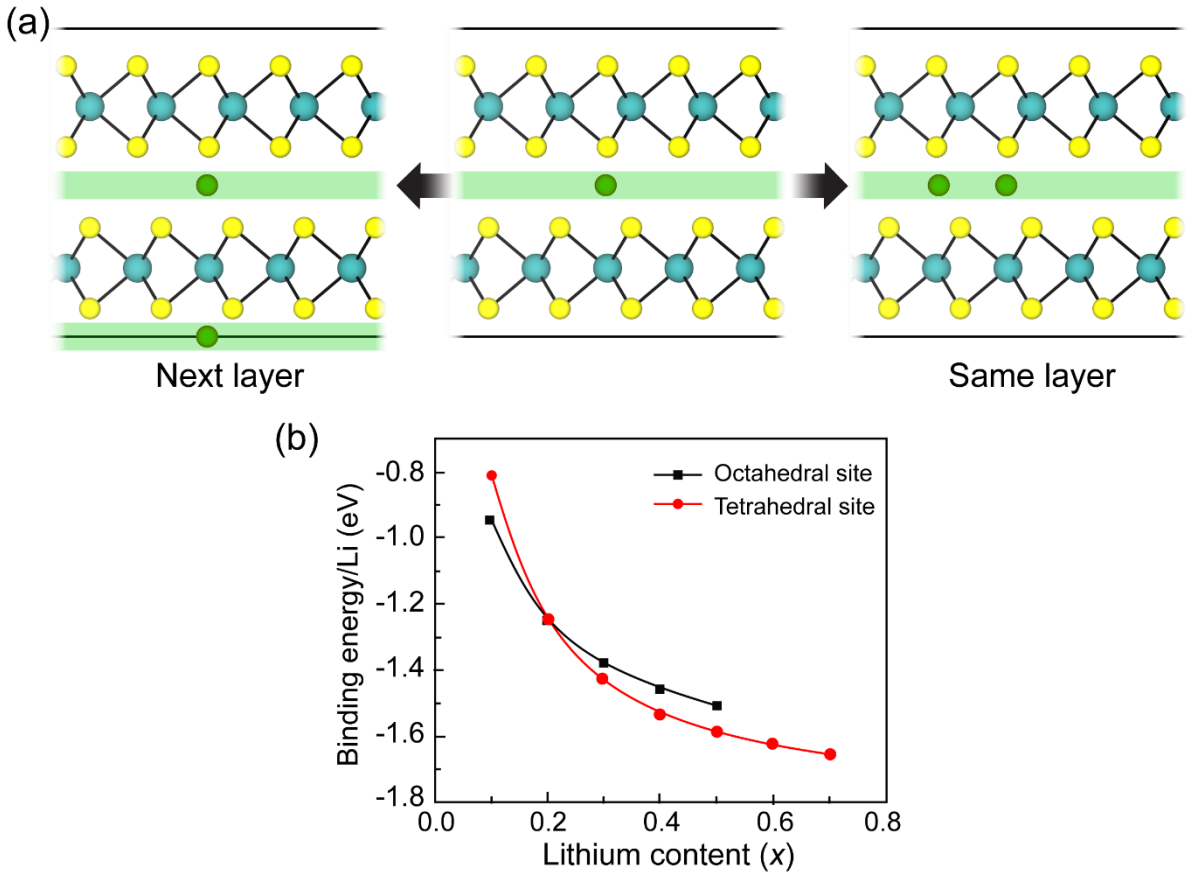

Figure 1: Schematic illustration for the scenario to investigate the intercalation behavior of a second Li-ion given an existing Li-ion at a T_d site (middle image). The second Li-ion can be intercalated at a tetrahedral (T_d) site in the same layer (right image) or next layer (left image). The green strips are added as a guide to the eye for Li-ions position. (b) Binding energy of Li as a function of Li content during sequential in-plane lithiation in the same interlayer spacing at octahedral (black) and tetrahedral (red) sites.

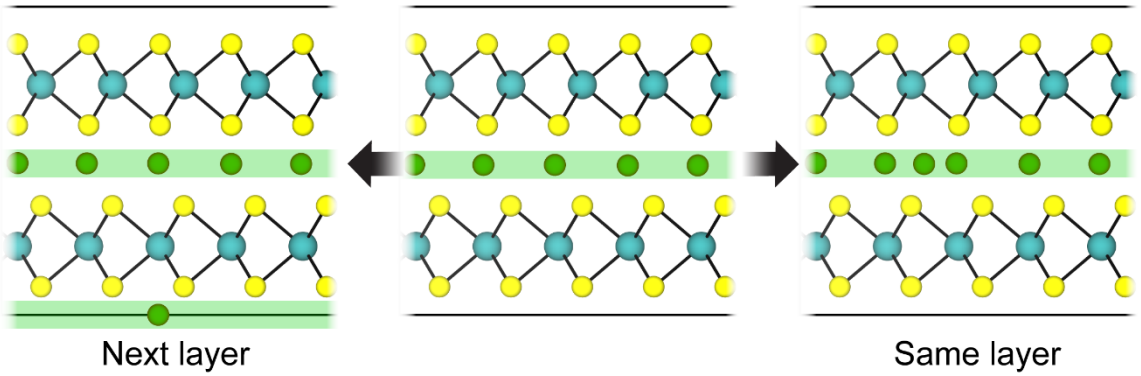

Figure 2: Schematic illustration for the absorption of Li-ions at an octahedral (O_h) site in the same layer (right) or next layer (left), when all the T_d sites in a layer are occupied. The green strips are added as a guide to the eye for Li-ions position.

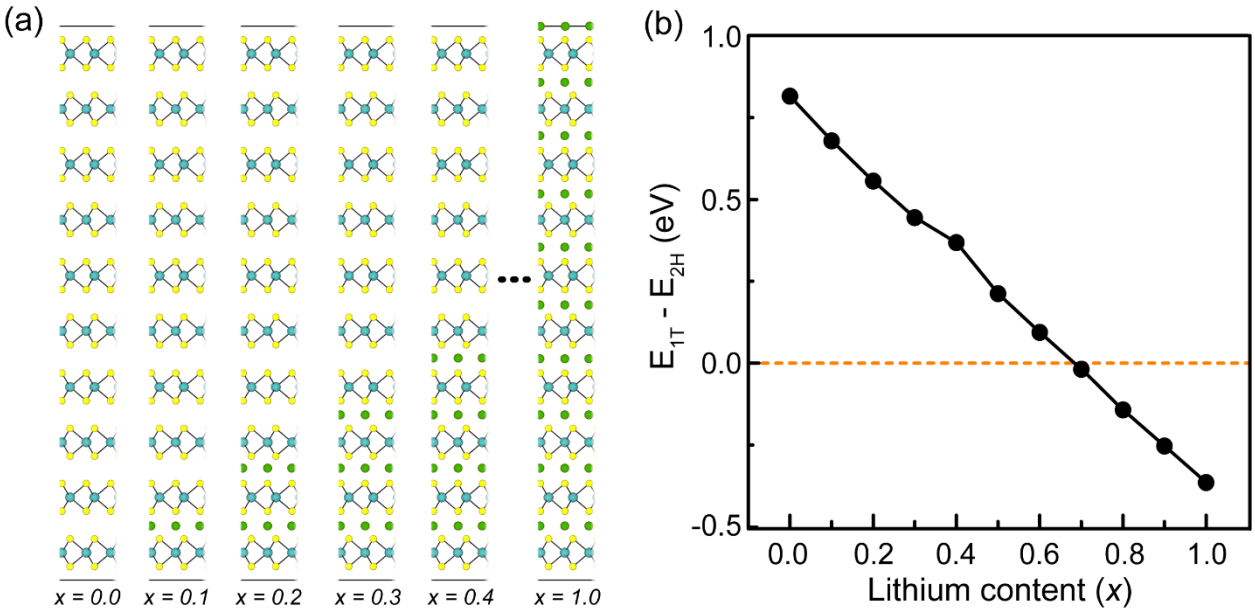

Figure 3: (a) Layer by layer lithiation of 2H-MoS_2 (xLi: MoS_2) with Li concentration increasing by 0.1 in each step and (b) the energy difference between lithiated 1T and 2H phases as a function of Li concentration. The dashed orange line shows that the phase transformation to 1T phase is energetically preferred after 0.7 concentration of Li.

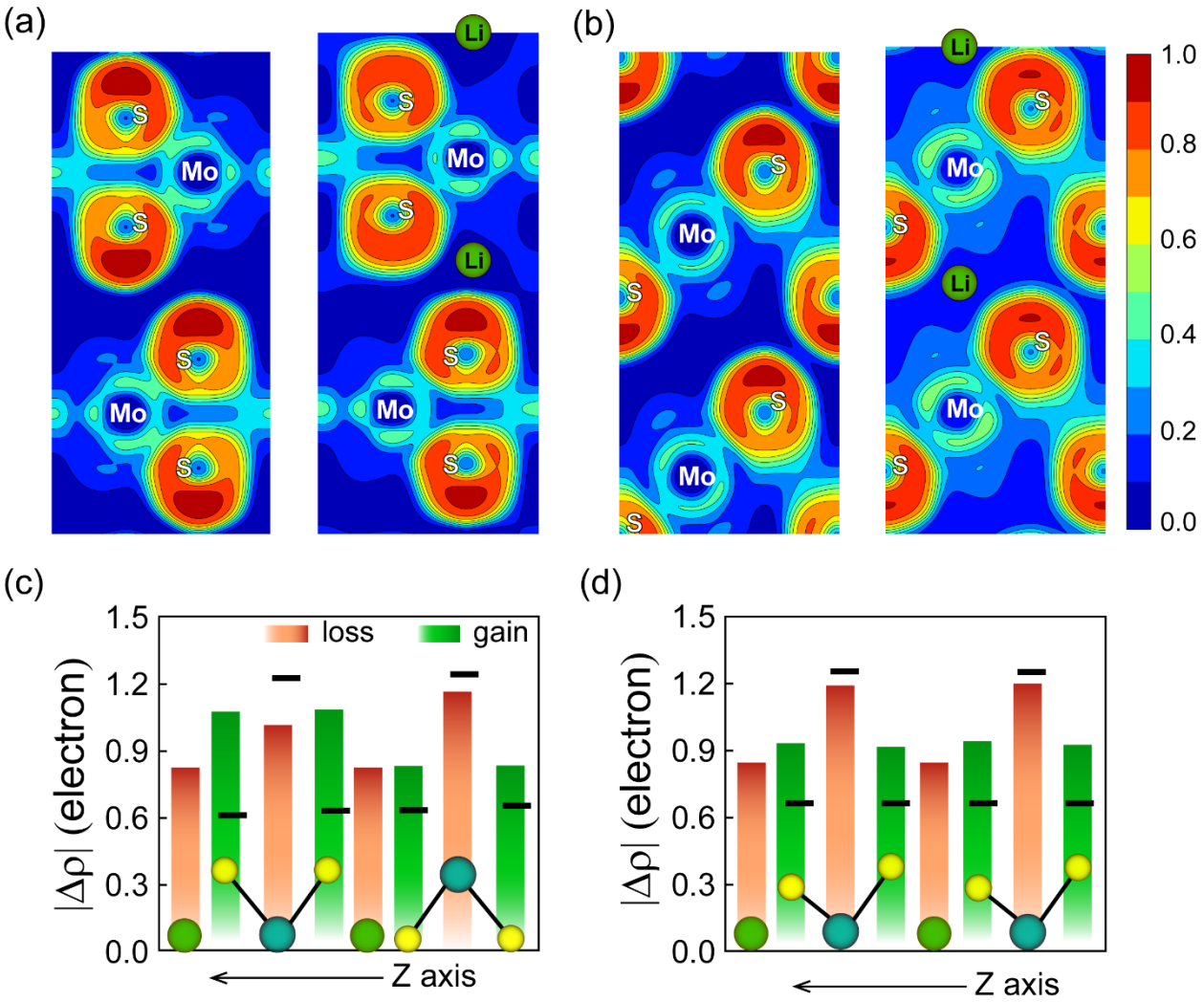

Figure 4: Electron localization function (ELF) projected on the [110] plane of the structure of unlithiated and lithiated (a) 2H and (b) 1T phases of MoS_2. Bader plots indicating charge transfer in (c) 2H and (d) 1T phases during lithiation of MoS_2.The orange and green bars show charge transfer from and to the atoms, respectively. The black horizontal lines represent the charge transfer in the case of unlithiated MoS_2.

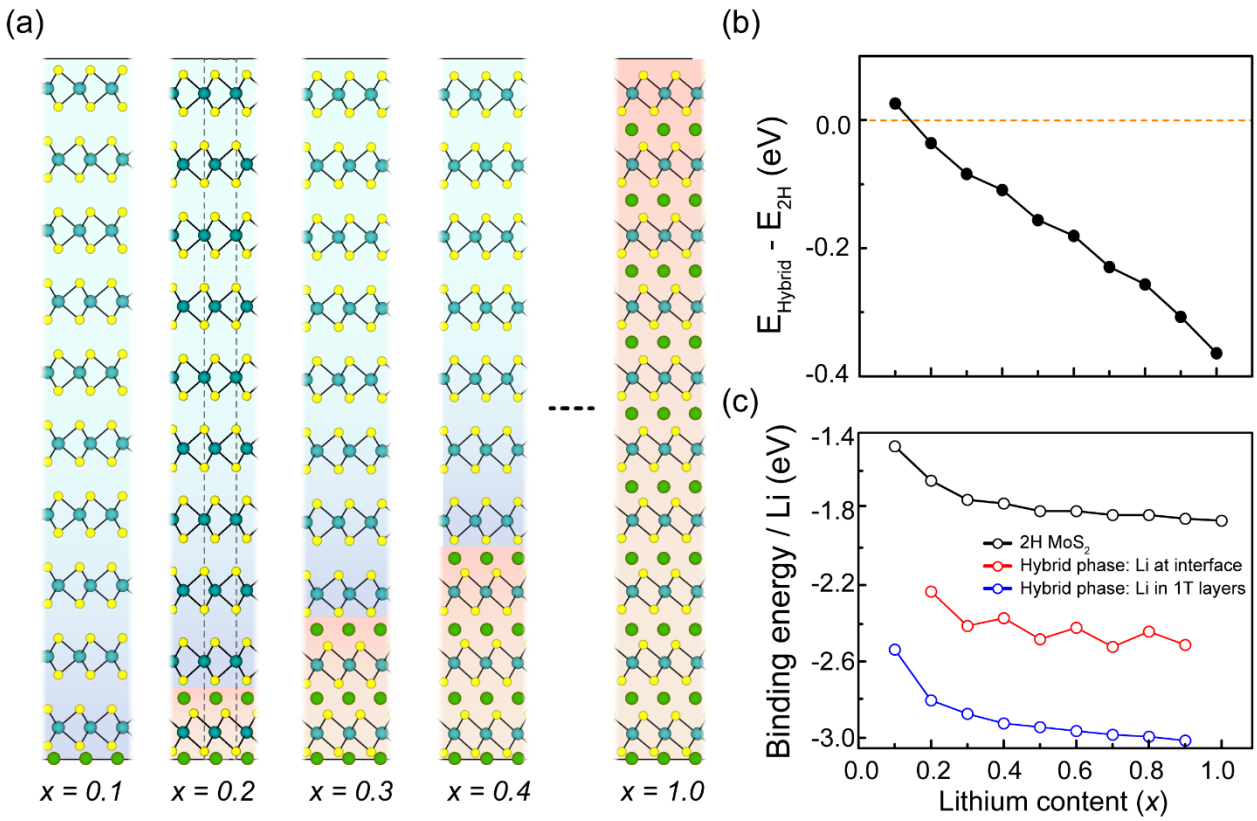

Figure 5: Layer by layer local phase transition in a 2H-1T hybrid structure with an increase in the concentration of Li. Orange and blue color slabs represent 1T and 2H phase of MoS_2, respectively. (The dotted lines provide guides to understand the position of Li at 2H-1T interface) (b) The energy difference between hybrid and 2H phases of MoS_2, showing local phase after 10% concentration of Li (xLi: MoS_2, x = 0.1), and (c) binding energy per Li-ion for 2H and hybrid structure (inside 1T and at the hybrid interface).

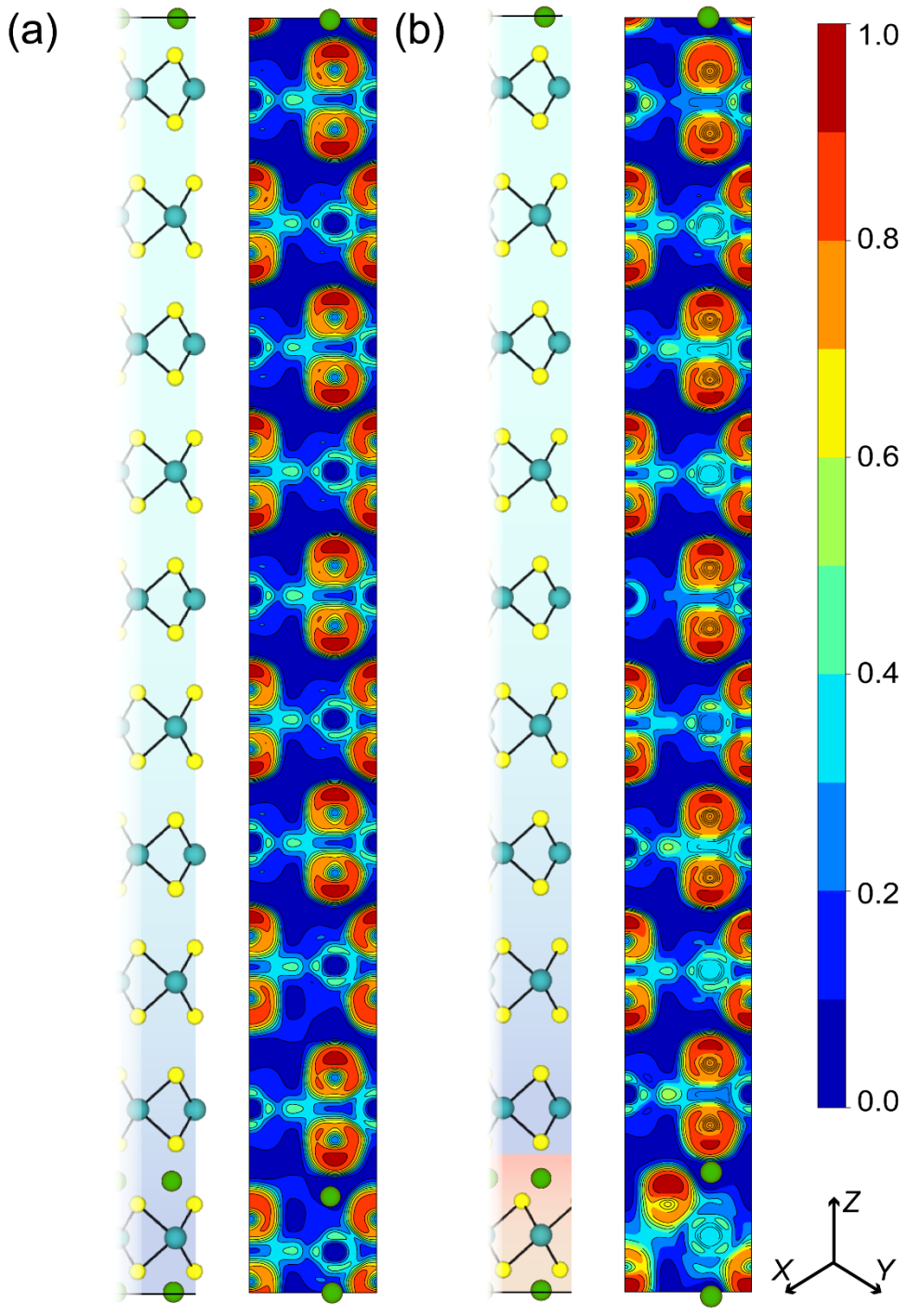

Figure 6: ELF for partially lithiated MoS_2 lattice (projected along (110) plane); left figure shows charge distribution without phase transformation while right shows the same following phase transformation of MoS_2 layer sandwiched between Li layers. Orange and blue color slabs represent 1T and 2H phase of MoS_2, respectively.

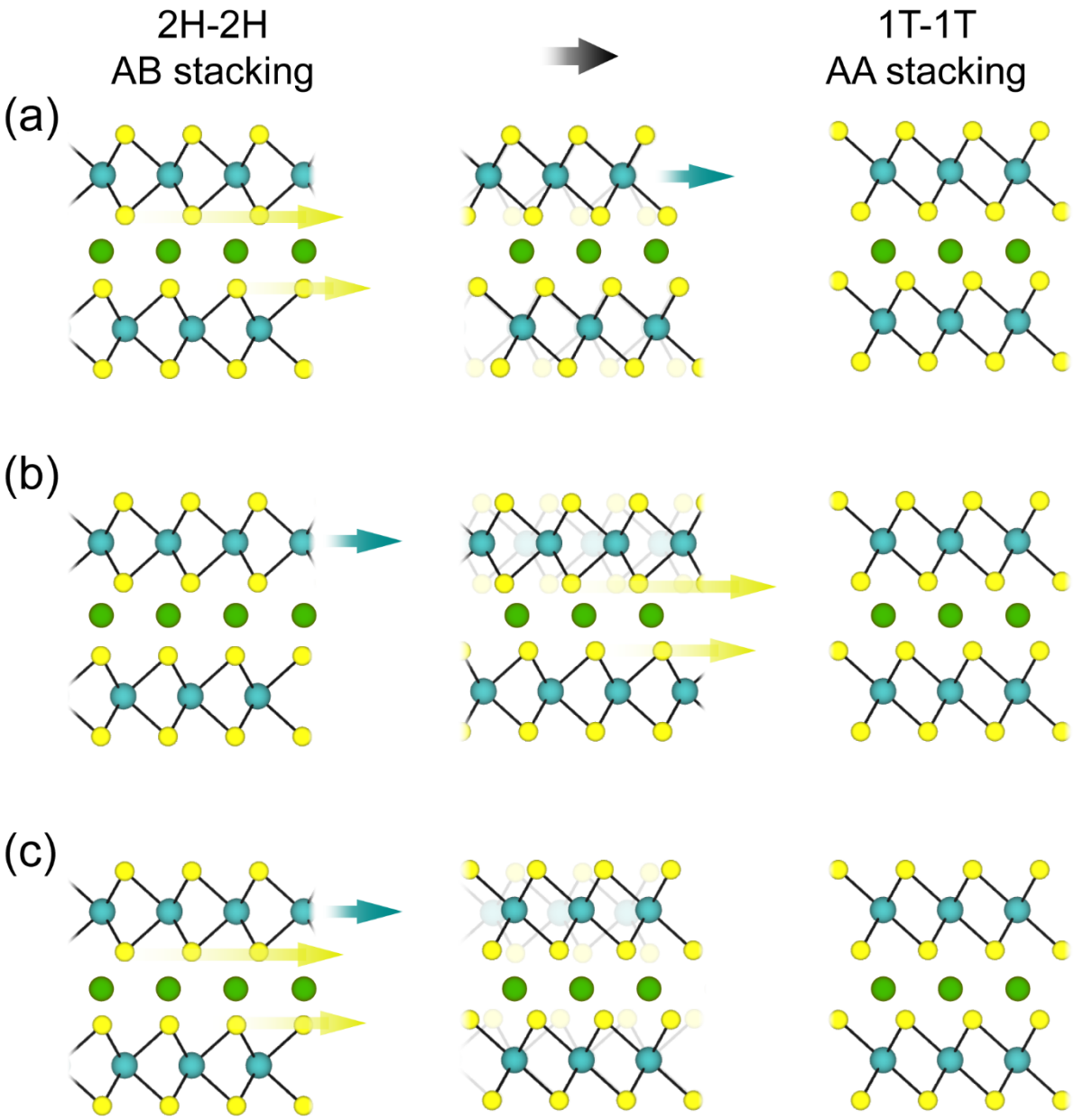

Figure 7: The possible routes for phase transformation from 2H-MoS_2 to 1T-MoS_2: (a) intralayer translation of S atoms, followed by change in interlayer stacking, (b) change in interlayer stacking and then translation of S atoms, and (c) both the phenomenon occurring together, respectively.

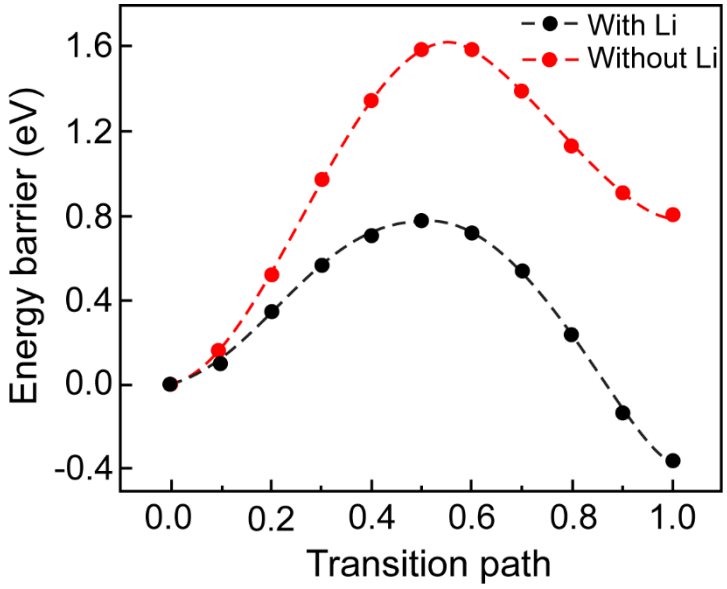

Figure 8: 2H to 1T phase transformation barrier with and without the presence of Li in between layers of MoS_2, comparing non-lithiated and fully lithiated systems.

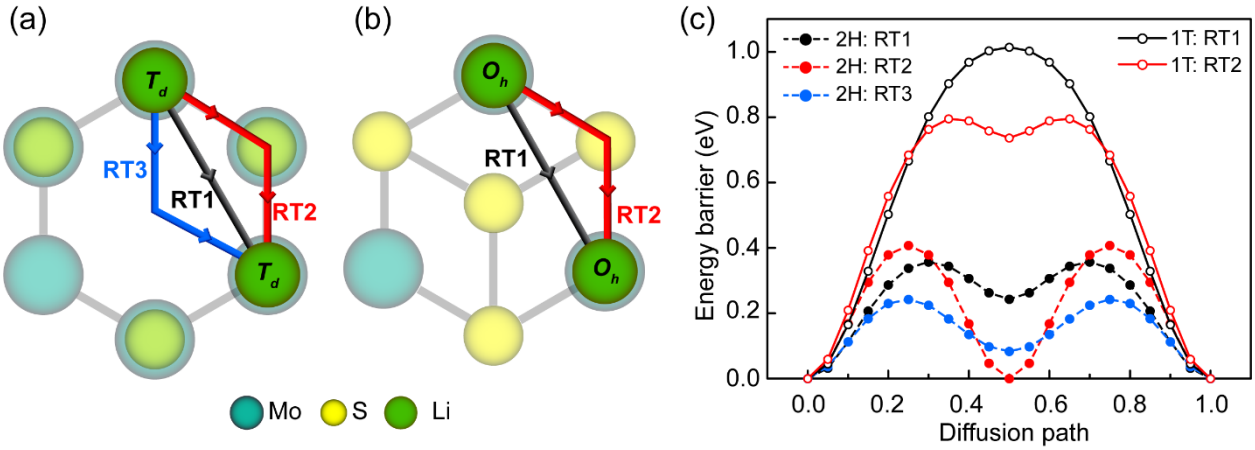

Figure 9: Schematic illustration of possible diffusion pathway for Li-ion in (a) 2H, (b) 1T-MoS_2, and (c) corresponding energy barrier (E_b). The MoS_2 structures are faded in the background to

highlight the paths. In 2H and 1T phases, atom diffuses from tetrahedral (T_d) and octahedral (O_h) sites, respectively.

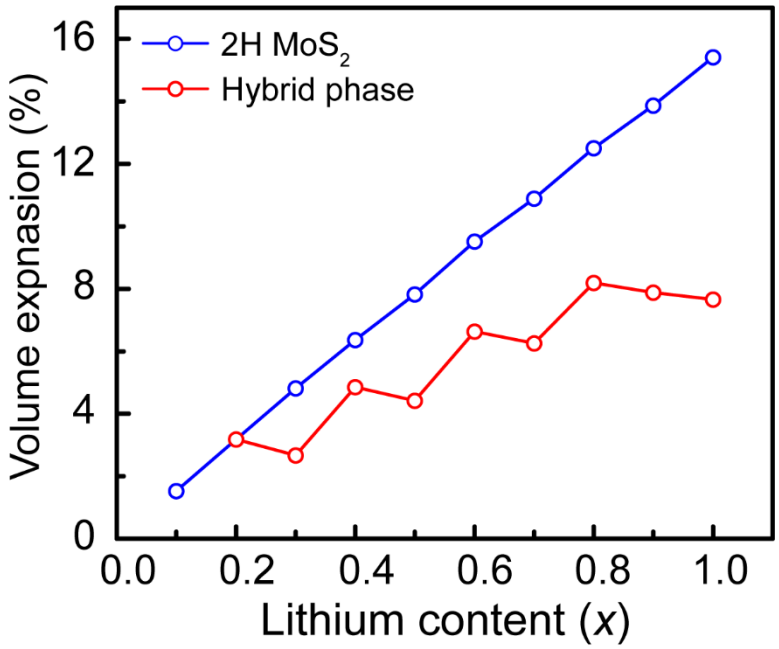

Figure 10: Volume expansion in 2H and hybrid structures with increasing concentration of Li-ions.